New Journal of Physics
The open access journal at the forefront of physics

PAPER • OPEN ACCESS

Linear polarization properties of energetic x-rays being Compton-scattered off atomic targets

IOP Publishing New J. Phys. 27 (2025) 073204 https://doi.org/10.1088/1367-2630/adf140

New Journal of Physics
The open access journal at the forefront of physics

Deutsche Physikalische Gesellschaft DPG
IOP Institute of Physics

Published in partnership with: Deutsche Physikalische Gesellschaft and the Institute of Physics

OPEN ACCESS

RECEIVED
4 April 2025

REVISED
14 July 2025

ACCEPTED FOR PUBLICATION
17 July 2025

PUBLISHED
30 July 2025

PAPER

Linear polarization properties of energetic x-rays being Compton-scattered off atomic targets

W Middents[1,2,3,*], A Gumberidze[1], T Krings[4], T Over-Winter[1,2,3], P Pfäfflein[1,2,3,5], N Schell[6], U Spillmann[1], M Vockert[1,2,3], G Weber[1,2,3] and Th Stöhlker[1,2,3]

[1] GSI Helmholtzzentrum für Schwerionenforschung GmbH, Planckstraße 1, D–64291 Darmstadt, Germany
[2] Helmholtz Institute Jena, Fröbelstieg 3, D–07743 Jena, Germany
[3] Institute of Optics and Quantum Electronics, Friedrich Schiller University Jena, Max-Wien-Platz 1, D–07743 Jena, Germany
[4] Institut für Kernphysik, Forschungszentrum Jülich, D–52425 Jülich, Germany
[5] European XFEL, Holzkoppel 4, Schenefeld D-22869, Germany
[6] Institute of Materials Physics, Helmholtz-Zentrum Hereon, Max-Planck-Str. 1, D–21502 Geesthacht, Germany
[*] Author to whom any correspondence should be addressed.

E-mail: wilko.middents@uni-jena.de

Keywords: Compton scattering, polarization transfer, impulse approximation, Compton polarimetry, x-ray scattering

Abstract

We perform a study on the Compton scattering of a photon beam off atomic targets. The main focus of this study is the influence of the momentum distribution of the target electrons on the polarization transfer in Compton scattering from the incident to the scattered photons. For this purpose we developed a Monte Carlo simulation of the Compton scattering process based on the relativistic impulse approximation. This simulation provides information on the double differential scattering cross section as well as the linear polarization of the scattered radiation over the entire energy range of the Compton peak for arbitrary incident linear polarization characteristics. Furthermore, we compare the predictions yielded by the simulation to data obtained in an experiment where a highly linearly polarized hard x-ray beam with a photon energy of 175 keV was scattered off a thin gold foil target. Both the simulation as well as the experimental results suggest a deviation of the linear polarization of the scattered radiation at the center of the Compton peak compared to scattering off a free electron at rest and a change of the polarization over the Compton peak due to the influence of the initial electron momentum.

1. Introduction

The inelastic scattering of a photon off an electron is referred to as Compton scattering, named after A. H. Compton, who first demonstrated this effect in 1923 [1, 2]. The incident photon of energy E scatters off the electron by transferring part of its energy to the electron. The scattered photon thus propagates with a reduced energy E' under the polar scattering angle θ. In the most basic picture of Compton scattering, the initial electron is assumed to be free and at rest. In this free electron approximation (FEA), the energy E' of the scattered photon is well defined by the incident photon energy and the polar scattering angle. The interaction cross section can be described by the Klein–Nishina-formula [3]. Including the polarization of the incident and scattered photons as well as the polarization of the electron, a more complete picture of the scattering process is provided by the transfer matrix formalism [4, 5].

For a realistic description of inelastic photon scattering off bound electrons, the electron cannot considered to be initially at rest, but its momentum density distribution needs to be taken into account. The impulse approximation (IA) [6–9] treats Compton scattering as the inelastic scattering of photons off an ensemble of free electrons with a momentum distribution according to the electron momentum density. The electron momentum distribution results in a Doppler broadening of the otherwise sharp energy of the scattered photon for a given observation angle, i.e. the so-called Compton profile. This model provides especially accurate results for scattering off weakly bound electrons, i.e. electrons in the higher atomic orbitals [10] resulting in energies of the scattered photon close to the center of the Compton profile [9].

However, a recent study highlights that, considering the emission of electrons in the Compton scattering process, even when the energy transfer in the scattering is much larger than the ionization energy of the electron in its initial state, the IA fails to reproduce all details of the Compton scattering process [11]. A more precise description of bound Compton scattering beyond the IA is provided by a scattering matrix approach [12, 13]. An overview of the various approaches to describe bound Compton scattering is found in [14], however in the present work we will focus on the IA approach.

While the double differential cross section (DDCS) of Compton scattering (differential in energy of the scattered photons ω' and in the solid angle Ω) is already well understood and described, so far a thorough investigation of the polarization transfer in the Compton scattering off bound electrons is missing. The present work addresses this gap by a consideration of the linear polarization of the incident and scattered radiation. A special focus is laid on the linear polarization of the scattered photon beam over the entire Compton profile and on the influence of the electron momentum distribution of the target atom on the polarization transfer from incident to scattered photon beam. For this purpose, a Monte Carlo simulation was developed which describes Compton scattering off an atomic target and provides information on the DDCS as well as the linear polarization of the scattered radiation over the entire Compton peak [15]. After an introduction into the basic physical concepts needed for this work in section 2, the simulation is described and discussed in section 3. In section 4 we present an experiment in which we investigate the scattering of a hard x-ray photon beam off a gold target and compare the results with our simulation in section 5.

2. Compton scattering of polarized photons

The basic concept of Compton scattering, taking into account the (linear) photon polarization is illustrated in figure 1. The incident photon of energy $\hbar\omega$ propagates along the z axis and scatters off an electron under the polar scattering angle θ with an azimuthal scattering angle ϕ between the x–z plane and the scattering plane (defined by the incident and outgoing photon directions). The scattered photon has a reduced energy $\hbar\omega'$ while the energy difference $\Delta E = \hbar\omega - \hbar\omega'$ is provided to the (recoil) electron. The energy of the scattered photon depends on the incident energy and the scattering angle θ

$$\hbar\omega' = \frac{\hbar\omega}{1 + \frac{\hbar\omega}{m_e c^2} \cdot (1 - \cos\theta)} \tag{1}$$

with m_e being the electron rest mass and c the speed of light. For unpolarized incident photons, the angular distribution of the scattered photons is provided by the Klein–Nishina formula [3] with r_e being the classical electron radius

$$\left(\frac{\mathrm{d}\sigma}{\mathrm{d}\Omega}\right)_{\mathrm{KN}} = \frac{r_e^2}{2} \cdot \left(\frac{\hbar\omega'}{\hbar\omega}\right)^2 \cdot \left(\frac{\hbar\omega'}{\hbar\omega} + \frac{\hbar\omega}{\hbar\omega'} - \sin^2\theta\right). \tag{2}$$

Including the polarization of the incident and scattered photons into the description provides a more complete picture of the scattering process. The polarization of a photon beam can be defined by the Stokes vector

$$\mathbf{P} = (1, P_1, P_2, P_3). \tag{3}$$

While the Stokes parameter P_3 describes the circular polarization of the photon beam and is not of interest in this study, the Stokes parameters P_1 and P_2 define the linear polarization of the photon beam. The Stokes parameters are closely related to the degree of linear polarization P_L and the polarization angle χ which is the orientation of the major polarization component with respect to a reference plane

$$P_1 = P_L \cdot \cos 2\chi \tag{4}$$

$$P_2 = P_L \cdot \sin 2\chi. \tag{5}$$

For the incident photon beam, the Stokes vector $\mathbf{P_i}$ is conveniently defined with respect to the x–z plane, while the Stokes vector of the scattered photon beam is defined with respect to the scattering plane spanned by the incident and scattered photon beam. For a scattering scenario, in which an incident photon beam with a certain linear polarization undergoes Compton scattering in the direction indicated by the polar and azimuthal scattering angles θ and ϕ, the scattering cross section and Stokes vector of the scattered photon beam can be calculated via the transfer matrix formalism [4]

$$\frac{\mathrm{d}\sigma}{\mathrm{d}\Omega} \cdot \mathbf{P_f} = \hat{T}(\theta) \cdot \hat{M}(\phi) \cdot \mathbf{P_i}. \tag{6}$$

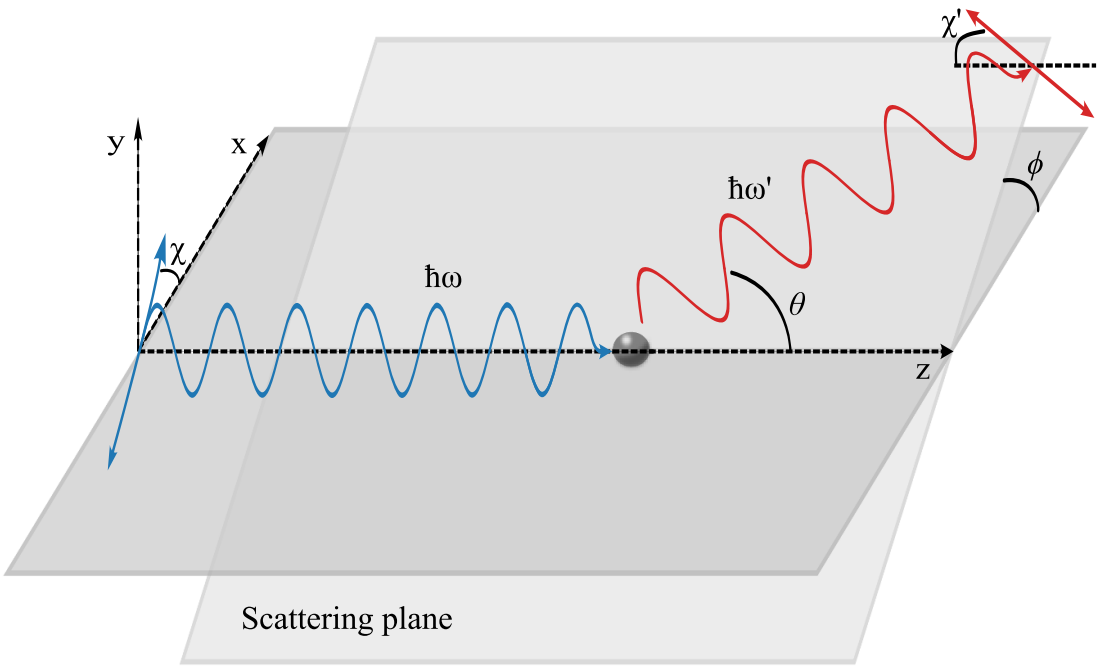

Figure 1. Concept of Compton scattering.

The rotation matrix $\hat{M}(\phi)$ transforms the Stokes vector of the incident photon beam into the scattering plane

$$\hat{M}(\phi) = \begin{pmatrix} 1 & 0 & 0 & 0 \\ 0 & \cos(2\phi) & \sin(2\phi) & 0 \\ 0 & -\sin(2\phi) & \cos(2\phi) & 0 \\ 0 & 0 & 0 & 1 \end{pmatrix}. \tag{7}$$

The scattering process itself is described in the transfer matrix $\hat{T}$. The individual components of the matrix include the scattering cross section and the polarization transfer from the incident to the scattered photon beam. For Compton scattering, the transfer matrix is given by [5]

$$\hat{T}(\theta) = \frac{r_e^2}{2} \cdot \left(\frac{\hbar\omega'}{\hbar\omega}\right)^2 \cdot \begin{pmatrix} \frac{\hbar\omega'}{\hbar\omega} + \frac{\hbar\omega}{\hbar\omega'} - \sin^2\theta & -\sin^2\theta & 0 & T_{03} \\ -\sin^2\theta & 1+\cos^2\theta & 0 & T_{13} \\ 0 & 0 & 2\cos\theta & T_{23} \\ T_{30} & T_{31} & T_{32} & T_{33} \end{pmatrix}. \tag{8}$$

The last row and column of the transfer matrix are related to the circular polarization of the incident and scattered photon beam. As the circular polarization is not investigated in this work, the exact expressions for these entries are not given in detail for better readability and can be neglected here. Except for T_{33} these entries depend on the spin-polarization of the target electron, which is (on average) 0 for atomic targets without external fields.

For the scattering off bound electrons, the electron binding properties and momentum distribution influence the scattering dynamics. In the IA, these influences can be treated as an integration over the electron momentum distribution to extract the DDCS of Compton scattering [14]. This concept is the basis of the simulation presented in the following chapter, where the DDCS and the Stokes parameters of the Compton scattered beam are calculated as a sum of the individual scattering events.

3. Simulation

The Compton scattering of an incident photon beam with a photon energy E_{in} off an atomic target is simulated [15]. For the simulation, it is assumed that the scattered photons are detected by an extended detector which is positioned at the polar and azimuthal observation angles θ and ϕ at a distance d from the scattering center. The simulation is performed according to the IA, meaning that for each individual simulation step the electron momentum is sampled from the electron momentum distribution (defined by

the bound electron wave function in the momentum space) and a photon beam scattering off electrons with this momentum is calculated. Thus, under the observation angle, defined by the detector position relative to the scattering center and the incident photon beam axis, the outgoing photon beams from different scattering geometries, defined by the specific electron momentum, are superimposed. This results in 'effective' DDCS and Stokes parameters for the scattered radiation which are obtained by a sum over the results for the cross section and Stokes parameters of the individual events. Three polarization states of the incident photon beam are considered for the simulation, being a fully linearly polarized beam with $P_{1,i} = 1$, a fully linearly polarized beam with $P_{2,i} = 1$ and an unpolarized incident photon beam ($P_{1,i} = P_{2,i} = 0$). This allows for a calculation of the scattering process for arbitrary linear polarization states by superposition of the 'pure' polarization states according to (6)

$$\begin{aligned}\left(\frac{\mathrm{d}^2\sigma}{\mathrm{d}\Omega\mathrm{d}\omega}\right)\cdot\mathbf{P_f} = (1-P_{1,i}-P_{2,i})\cdot\left(\frac{\mathrm{d}^2\sigma}{\mathrm{d}\Omega\mathrm{d}\omega}\right)_{P_i=0}\cdot\mathbf{P_{f,P_i=0}}\\ +P_{1,i}\cdot\left(\frac{\mathrm{d}^2\sigma}{\mathrm{d}\Omega\mathrm{d}\omega}\right)_{P_{1,i}=1}\cdot\mathbf{P_{f,P_{1,i}=1}}\\ +P_{2,i}\cdot\left(\frac{\mathrm{d}^2\sigma}{\mathrm{d}\Omega\mathrm{d}\omega}\right)_{P_{2,i}=1}\cdot\mathbf{P_{f,P_{2,i}=1}}.\end{aligned} \tag{9}$$

In the simulation, n scattering events are simulated. For each of these events, the following process is repeated for the three polarization states of the incident photon beam.

The incident photon beam obtains an energy E which is chosen within a certain energy range dE around the center energy E_{in}. The polar and azimuthal scattering angles θ and ϕ in the laboratory frame are varied according to the opening angle defined by the detector geometry. For the electron off which the photon beam scatters, an electron orbital is chosen at random, considering the corresponding numbers of electrons in each orbital. From this, the electron is attributed with a momentum according to the electron momentum density distribution in the corresponding orbital [16, 17]. The electron momentum is distributed randomly into its x-, y- and z-components.

The Compton scattering is calculated in the electron rest frame. As the Stokes vector for a photon beam propagating in the x–z plane is invariant under a Lorentz transformation along the x axis [18], first the system is rotated such, that the electron momentum in the rotated system is solely oriented along the x axis and the incident photon propagates in the x–z plane. Then, the system is Lorentz transformed into the electron rest frame. This transformation results in a red- or blueshift of the photon energy and a transformation of the scattering angles depending on the (orientation and absolute value of the) sampled electron momentum.

In the electron rest frame, the scattering process can be treated as Compton scattering off free electrons. The energy relation between the incident and the scattered photon beam is calculated according to (1). The differential scattering cross section and the Stokes vector of the scattered photon beam are determined via the transfer matrix formalism (equations (6)–(8)). Note, that as by the transformation to the electron rest frame the scattering angles and the incident photon energy are varied depending on the sampled electron momentum, this means, that the polarization of the scattered photon is influenced by the sampled electron momentum.

After calculation of the scattering event, the system is transformed back to the laboratory system. For this, again a rotation is performed such, that the scattering plane is the x–z plane and the back transformation is along the x axis. Afterwards a Lorentz transformation to the (rotated) laboratory system is performed. While the Stokes vector does not change under the Lorentz transformation, the scattering cross section is boosted according to [19]

$$\frac{\mathrm{d}\sigma}{\mathrm{d}\omega} = \frac{1}{\gamma^2\cdot(1-\beta\cos\theta)^2}\cdot\frac{\mathrm{d}\sigma'}{\mathrm{d}\Omega'}, \tag{10}$$

where the primed coordinates correspond to the electron rest frame and the unprimed ones correspond to the laboratory frame. Here, β is the ratio of the electron velocity to the speed of light and γ is the relativistic Lorentz factor. Additionally, the energy of the Compton scattered photon is red- or blue-shifted in the transformation from the electron rest frame to the laboratory frame. Since for inelastic scattering off a bound electron, the transferred energy needs to surpass the corresponding binding energy, the energy difference between incident and scattered photon in the laboratory frame is checked. Events which do not fulfill this condition are discarded.

After the transformation back into the laboratory frame, a final rotation of the system is performed in order to orient the scattered photon beam along the z axis and the incident photon beam within the x–z

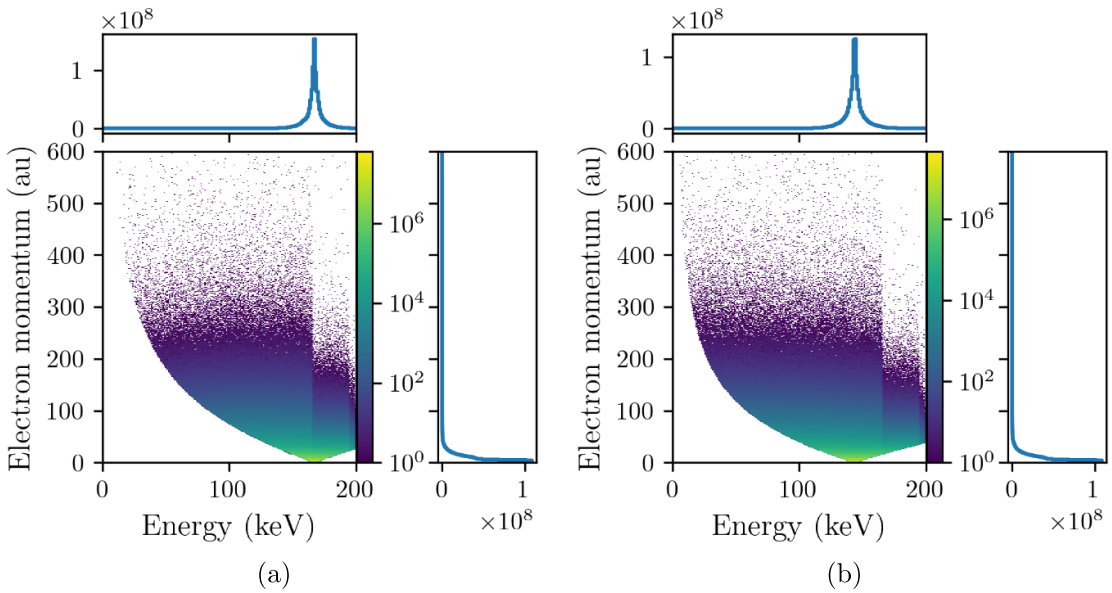

Figure 2. Spread of the resulting energy of the Compton scattered photons depending on the electron momentum. 10^9 photons with an incident photon energy of 200 keV and a linewidth of dE = .25 keV were simulated scattering off a Xenon atom and observed under (a) $\theta = 60°$ and (b) $\theta = 90°$. For an explanation of the pronounced edges visible in both data sets at 165.4 keV and 194.6 keV see text.

plane. Finally, the results for the cross section and for the Stokes parameters $P_{1,f}$ and $P_{2,f}$ of the scattered photon beam are stored on an energy-resolved array, separately for the individual electron orbitals.

The energy resolved DDCS for each orbital is calculated as a sum of the individual events, normalized to the total amount of events in the orbital and the energy-width of the arrays. Additionally, the result needs to be multiplied by the amount of contributing electrons in the respected orbital. Similarly, the behavior of the Stokes parameters can be calculated as a sum of the product of the individual Stokes parameters and the corresponding cross section, normalized to the summed values of the cross sections. The complete energy resolved DDCS and Stokes parameters for scattering off the entire atom is given by the sum of the individual contributions from each orbital.

Figure 2 shows the dependence of the energy of the Compton scattered photons on the momentum of the bound electron. The simulation was performed with $n = 10^9$ photons with an incident photon energy $E_{\text{in}} = 200\,\text{keV}$ in an energy range of d$E = 0.25\,\text{keV}$ scattering off a Xenon atom ($Z = 54$). The scattered radiation was observed under (a) $\theta = 60°$ and (b) $\theta = 90°$ with a point-like opening angle. As expected, most simulated electrons carry only small momenta due to the momentum density distribution. For these scattering scenarios, the scattered photon energy will only vary slightly from scattering off a free electron with no momentum as only small Doppler corrections are possible. With increasing electron momenta, also scattering scenarios with increasing variations of the scattered photon energy become possible. As only scattering events where the difference between incident and scattered photon energy exceeds the binding energy of the electron can contribute to bound Compton scattering, abrupt steps in the amount of events contributing to a certain scattered photon energy occur, where the energy condition is not fulfilled for certain electron orbitals. For instance, the pronounced edge visible in both data sets at 165.4 keV are due to the K edge ionization potential introducing a cutoff for K shell electrons to contribute to Compton scattering.

As the scattered photon energy depends both on the absolute value and orientation of the electron momentum, different absolute electron momenta can lead to the same scattered photon energy. Thus, the DDCS and polarization characteristics of the scattered photon beam at certain energies across the Compton peak are the superposition of the individual scattering cross sections and polarization states for these different scattering scenarios. The resulting DDCS and linear polarization of the scattered photon beam across the Compton peak for the simulated parameters used in figure 2 are presented in figures 3 and 4. As expected, the cross section strongly decreases towards the tails of the Compton peak since the probability of the electron carrying a sufficient momentum also decreases towards these regions. This also results in the increased noise especially in the polarization values, as only few events were calculated with the simulation settings in this regime. Additionally, at energies, where the binding energy exceeds the difference between incident and scattered photon energy ($E_f \approx 165\,\text{keV}$ for the K-shell and $E_f \approx 195\,\text{keV}$ for the L-shell) a sharp decrease of the cross section is visible. The simulation results for the DDCS are compared to an analytical calculation

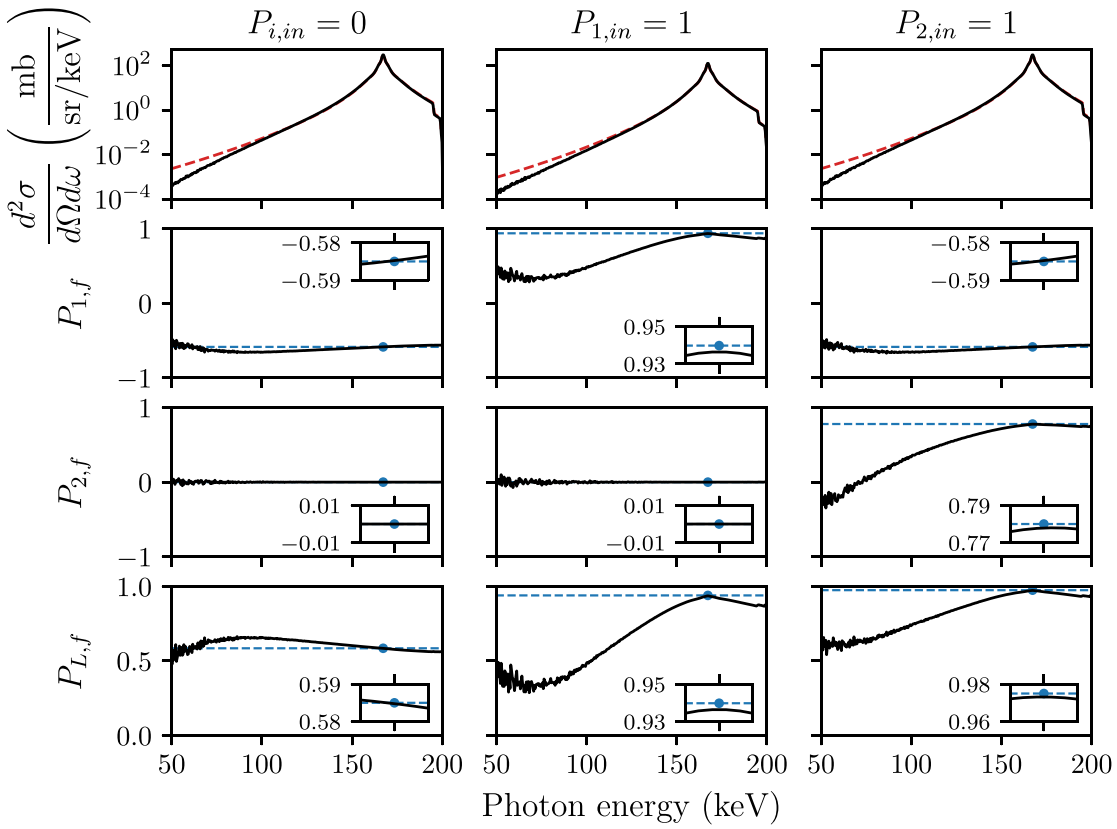

Figure 3. Simulated results (black) for the Compton scattering of a 200 keV photon beam off Xenon atoms under $\theta = 60°$, $\phi = 0$ with $n = 10^9$ photons. The top row shows the DDCS compared to results from an analytical calculation based on the relativistic IA (red). The lower three rows present the Stokes parameters $P_{1,f}$, $P_{2,f}$ and the degree of linear polarization $P_{L,f}$ compared to the FEA (blue dot and dashed line). The individual columns show the results for $P_{1,i} = P_{2,i} = 0$, $P_{1,i} = 1$ and $P_{2,i} = 1$. The inserted plots show a zoom of the center of the Compton peak ± 1 keV.

using the relativistic IA as proposed by Ribberfors [8]. For our implementation of this treatment we followed equations (30) to (41) in [20]. Both, the simulated behavior and the analytical model show similar results, especially at the center of the Compton peak, confirming the validity of the simulation. However, towards the tails of the Compton peak, the results of the simulation and the standard relativistic IA calculation deviate. This deviation is best seen in the case of a fully linearly polarized photon beam scattering at $\theta = 90°$, $\phi = 0$. The reason for this behavior is twofold: first, within the relativistic IA calculation only the electron momentum projection p_z on the scattering vector between incident and scattered photon beam is used [21], while the simulation treats the entire three dimensional electron momentum. Second, in the treatment by Ribberfors, the (linear) polarization of the incident photon beam is not considered. To account for polarized radiation, we used the polarization-dependent variant of the DDCS in our implementation of the relativistic IA. The deviation between simulation and analytical calculation are most pronounced for a polarized beam and an observation angle of $\theta = 90°$ as here the expected scattering cross section gets minimal for an incident photon energy of $E_{\text{in}} = 200$ keV. This effect is easy to understand in the limit of Thomson scattering, where the scattering cross section under $\theta = 90°$, $\phi = 0$ is zero for 100% linear polarization of the incident photon beam while any deviation from this scattering angle due to a non-vanishing initial electron momentum results in a non-zero cross section. Thus, in this situation all radiation that is detected under an observation angle of 90° is expected to originate from scattering geometries where theta is unequal 90°. In a similar way, the effect of non-vanishing electron momentum on the observed scattered radiation is most pronounced when the DDCS for the case of zero electron momentum is minimal.

Also the polarization of the scattered photons shows a distinct pattern across the Compton peak, dependent on the polarization state of the incident photon beam. If the incident photon beam is unpolarized or for co-planar scattering geometries, where the scattering plane coincides with the polarization plane of the incident photon beam, the scattered photon beam will also be only polarized parallel or perpendicular to the scattering plane. Thus, for this geometry $P_{2,f} = 0$ across the entire Compton peak, as is also expected for Compton scattering off a free electron in this geometry. Otherwise, the polarization of the scattered photon beam will vary across the Compton peak. Curiously, even at the center of the Compton peak, the

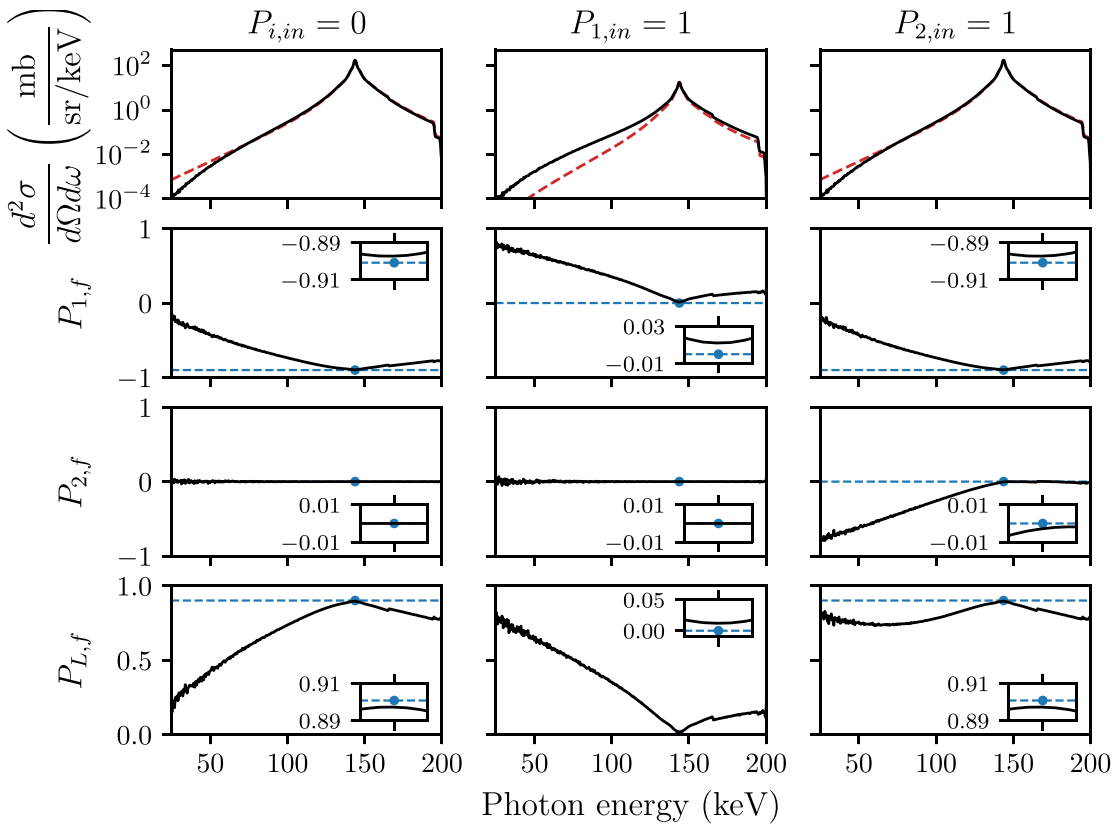

Figure 4. Same as figure 3 for $\theta = 90°$, $\phi = 0°$.

polarization of the scattered photons slightly varies compared to scattering off a free electron. This behavior stems from the influence of the higher momenta electrons, which is at the center small but still visible and leads to a slight change in polarization of the scattered photon beam. Additionally, not only a depolarization of the scattered photon beam is possible, but the Stokes parameters can also be increased, depending on the exact scattering scenario (θ, ϕ, $\mathbf{P_{in}}$, E_{in}). As for the DDCS, also the Stokes parameters show distinct steps at the energies related to certain electron shells. This hints to distinct polarization features for Compton scattering off the individual electron orbitals.

Figure 5 shows the DDCS and the Stokes parameter $P_{1,f}$ resolved for the individual electron shells for scattering both an unpolarized and a fully polarized photon beam of energy $E_{\text{in}} = 200\,\text{keV}$ observed under $\theta = 90°$, $\phi = 0°$. Again, it is clearly visible, that the electron shells only contribute, if the energy difference between incident and scattered photon is sufficient. The center of the Compton peak is dominated by scattering off the loosely bound electrons in the higher shells. Vice versa, the influence of the electrons from more strongly bound shells becomes dominant for an increasing distance from the maximum of the Compton peak. This correlates to the higher probability of the lower shell electrons to carry a higher momentum. Regarding the polarization of the scattered photon beam in the peak center, contributions from the higher shells show behavior close to the scattering off a free electron. However, the contribution from inner electron shells, stemming on average from higher electron momenta, leads to stronger deviations from the FEA. While these parts only contribute slightly due to their relatively small cross section in the center region, the strong deviation can explain the overall observed deviation at the Compton peak center.

4. Experiment

In an experiment at the High Energy Materials Science Beamline P07 [22] of the third generation synchrotron facility PETRA III @ DESY in Hamburg, a photon beam with a photon energy of $E_{\text{in}} = 175\,\text{keV}$ was scattered off a gold foil target. The experiment is described in detail in [23]. From an analysis of the angular distribution of Rayleigh scattering in this experiment, the Stokes parameters of linear polarization of the synchrotron beam were determined to be $P_{1,i} = 0.988 \pm 0.004$ and $P_{2,i} = 0.023 \pm 0.047$.

In this work, we focus on the radiation being Compton-scattered off the gold target and detected by a double-sided segmented silicon crystal detector [24]. The used detector was positioned under different polar

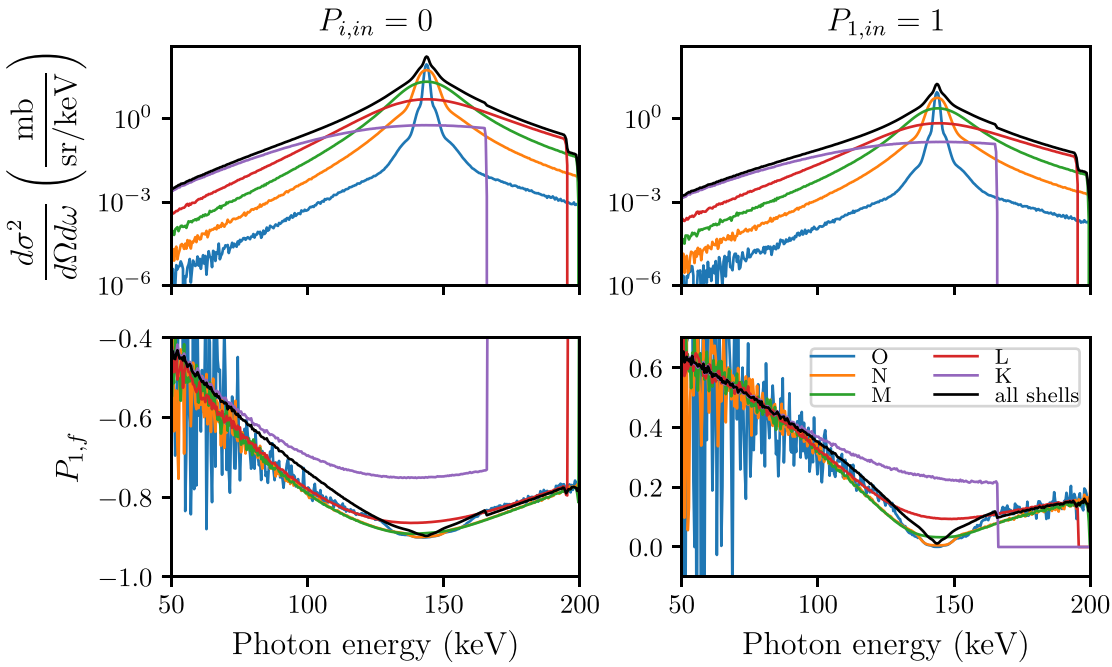

Figure 5. Compton scattering of a photon beam with an energy of $E_{\text{in}} = 200\,\text{keV}$ off the individual electron shells of a Xe atom observed under $\theta = 90°$, $\phi = 0$. The upper row shows the DDCS and the lower row the Stokes parameter $P_{1,f}$.

Table 1. Different positions of the Compton polarimeter used in the experiment at PETRA III [23].

θ	63.4°	65.2°	88.2°	71.7°	89.1°
ϕ	0	158°	161°	133°	136°

and azimuthal scattering angles, see table 1. In particular, the linear polarization of the Compton scattered radiation is analyzed. For this purpose, the used detector can serve as an energy–resolving Compton polarimeter in an energy range of 50 keV–200 keV. The determination of the linear polarization of the analyzed radiation here is based on events, where the detected photons are not directly photoabsorbed but are Compton scattered within the detector and subsequently the scattered photons are also detected at another position on the detector. The resulting azimuthal scattering pattern of these events will follow the azimuthal scattering cross section of Compton scattering and thus allows for a precise determination of the linear polarization of the investigated radiation [25]. For an in-depth description of the Compton polarimetry technique in general [26] and of the Compton polarimetry based on double-sided segmented semiconductor crystal detector in particular [25, 27, 28]. Note, that we analyze the photon beam being Compton scattered off the gold target and for the determination of the linear polarization of the scattered photon beam, we analyze events, were additionally full Compton scattering events within the detector crystal are registered.

The energy–resolved spectra are obtained from direct photo-absorption events in the detector (indicated by a single energy deposition within the detector crystal). Figure 6 shows a calibrated example energy spectrum obtained with the Compton polarimeter positioned at observation angles of $\theta = 89.1°$, $\phi = 136°$ in an energy range between 60 keV–180 keV. The spectrum results from averaging the energy information from the front side contacts and the backside contacts of the detector crystal. The energy resolution of the detector can be estimated from the Rayleigh peak, assuming a Gaussian peak profile including correction terms, similar to the procedure performed in [23]. Here, for simplicity only a step function in the detector response is assumed as correction term. From an adjustment of a Gaussian peak shape plus the step function, a detector resolution of $\approx 1.7\,\text{keV}$ FWHM is determined.

The linear polarization of the detected photons can be determined from the double–hit events on the detector (i.e. two separated energy depositions at different positions in the detector per event). These can be events corresponding to Compton scattering within the detector crystal where one deposition corresponds to the energy loss in scattering, i.e. the recoil electron while the second deposition corresponds to the photo absorption of the scattered photon. Combining information on the energy and position of these events, the azimuthal Compton scattering distribution in the detector is reconstructed. Following (1), the double-hit events can be filtered for true Compton events and the individual energy depositions can be attributed to be the scattering position or the photo absorption of the scattered photon. As Compton scattering is anisotropic

and preferentially perpendicular to the polarization direction of the incident radiation (see equations (6)–(8)), from the (azimuthal) scattering distribution, the linear polarization, i.e. the Stokes parameters P_1 and P_2, of the analyzed radiation can be determined. Note, that we analyze the radiation that was previously Compton scattered off the gold foil target and now undergoes subsequent Compton scattering on the detector for the polarimetry.

Similar to the approach used in [29], our reconstruction algorithm for the polarization of the analyzed radiation is based on a fitting of a linear combination of Monte Carlo simulated scattering distributions with fixed polarization state of the incident radiation to the experimental data. Based on the orientation of the polarization of the scattered photon beam, the polarization states for the model distributions are chosen from a set of fully polarized light being oriented under either $\chi = 0°$ ($I_{0°}$) or $\chi = 90°$ ($I_{90°}$) and either $\chi = 45°$ ($I_{45°}$) or $\chi = 135°$ ($I_{135°}$) and completely depolarized light (I_0). The simulated model distributions are obtained from a simulation based on an EGS5 Monte Carlo code for photon and electron transport in matter [30, 31]. These model distributions are superimposed with the Stokes parameters of the radiation $P_{1,i}$ and $P_{2,i}$ as free parameters. The fitting procedure is performed with the iminuit package [32]. For an estimation of the uncertainties in the fitting parameters, i.e. the Stokes parameters, the Minuit.hesse() function is used, providing asymptotic errors according to the Hesse matrix approach. To avoid systematic errors due to binning effect, the fitting is repeated for different bin-sizes of the scattering distributions. Additionally, for estimating the statistical uncertainty of the simulated distributions, for each of these steps a bootstrapping approach is used to resample these.

This method is performed for different energies across the Compton peak. For this, only double-hit events with a summed energy in a certain energy window are used to reconstruct the Compton scattering distribution within the detector. In our analysis, we set the energy window to be ± 1.5 keV as a trade-off between good statistics and still low broadening effects due to the change in polarization with energy.

5. Results and discussion

First, the energy–resolved spectrum in figure 6 is investigated. The center energy of the broad Compton peak from inelastic scattering off the foil target depends on the polar scattering angle θ. For the shown spectrum, the center of the Compton peak is at 131 keV. For an analysis of the Compton peak, each of the scattering scenarios from table 1 is simulated with the simulation described in section 3 with $n = 10^8$ photons. The results for the DDCS are folded with a Gaussian to match the resolution of the detector and corrected by the efficiency of the detector. The efficiency curves are obtained by the same code based on EGS5 as described in the previous section. For a fit of the DDCS to the experimental spectra additionally a constant offset and, similarly to the fit of the Rayleigh peak, a step function in the detector response is assumed (both also efficiency corrected). The fitted intensity profile shows an excellent agreement with the measured spectrum over a broad energy range for each measurement position. Especially, the high energy tail of the Compton peak is well described by the simulated DDCS, even up to the elastic scattering peak. On the low energy side of the peak, the DDCS fit matches the peak structure of the Compton peak well over a broad energy range (here over 10 keV from the peak center). The deviation between the measured spectrum and the fit far from the peak center can probably be explained by the background of unknown shape and origin in the spectrum and the simplifications in modeling the detector response.

The total intensity of the Compton scattering peak can be extracted for each measurement by integrating the fitted intensity profile over the scattered photon energy. From this, an estimation of the angle-DDCS of Compton scattering can be performed based on the ratio of the intensities of the Compton peak and the elastic (Rayleigh) scattering peak. For obtaining this relative cross section, the necessary angle-differential cross sections of Rayleigh scattering are provided in [23], where a similar method was used. Especially for the broad Compton peak, the detector response can not be estimated well across the entire energy range, thus for the determination of the intensities of the Compton and Rayleigh peaks, the detector response is ignored and only the terms for the peak profiles are considered. This is justifiable, since the response terms provide only minor corrections to the total intensities. Additionally, the expected angle-DDCSs for Compton scattering can be determined by an integration of the DDCS provided by the simulation over the scattered photon energy. For this, an incident linear polarization of $P_{1,i} = 0.99$ is assumed. The angle-DDCSs are presented in table 2. From this comparison already a good agreement between experiment and simulation can be seen. Additionally, the expected cross section for the FEA based on (6) (multiplied by the number of electrons $Z = 79$) is presented. As expected, the FEA results slightly vary from the simulation and show on average a stronger disagreement with the experimental values.

The Stokes parameters P_1 and P_2 for the Compton scattered radiation in the center of the Compton peak are presented in table 3. Next to the experimental results, the expected values are shown both for a calculation in the FEA and results extracted from the simulation. The uncertainties in the values obtained

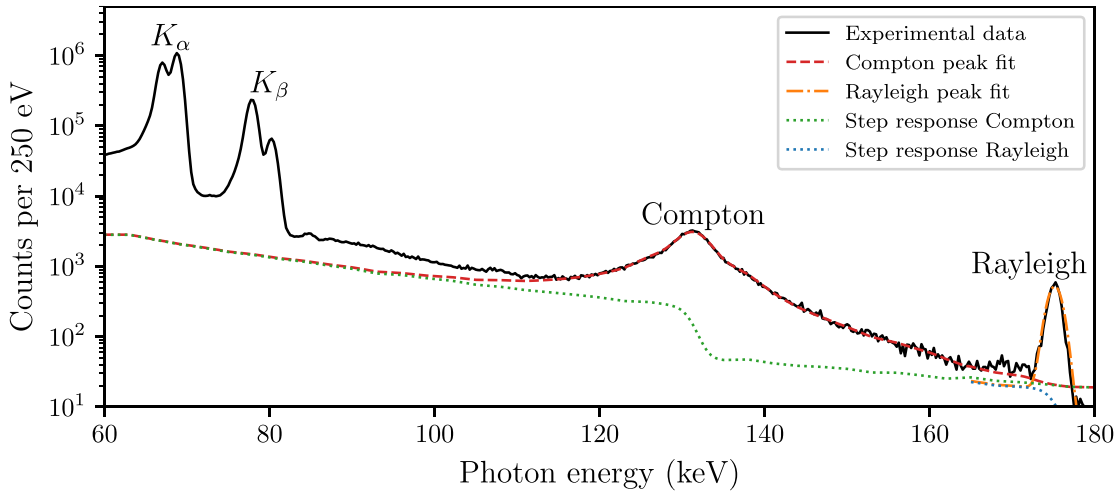

Figure 6. Energy spectrum obtained from scattering 175 keV photons off a gold target at $\theta = 89.1°$, $\phi = 136°$. The individual components are labeled.

Table 2. Angle-differential cross sections of Compton scattering off gold atoms. The cross sections are presented in mb sr^{-1}.

(θ, ϕ)	Experiment	Simulation	FEA
$(63.4°, 0)$	901 ± 42	945	976
$(65.2°, 158°)$	1168 ± 61	1299	1361
$(88.2°, 161°)$	577 ± 53	555	538
$(71.7°, 133°)$	2245 ± 69	2351	2491
$(89.1°, 136°)$	1620 ± 83	1790	1846

Table 3. Stokes parameters P_1 and P_2 for the Compton scattered photon beam in the center of the Compton peak. The experimental values (exp) are compared to both estimated Stokes parameters resulting from a calculation in the FEA and values resulting from the simulation (sim). The uncertainty in the simulation stems from the uncertainty in the incident photon polarization, for the FEA values also uncertainties in the scattering angles θ and ϕ are included.

(θ, ϕ)	$P_{1,\mathrm{FEA}}$	$P_{2,\mathrm{FEA}}$	$P_{1,\mathrm{sim}}$	$P_{2,\mathrm{sim}}$	$P_{1,\mathrm{exp}}$	$P_{2,\mathrm{exp}}$
$(63.4°, 0)$	+0.877(17)	+0.047(96)	+0.877(25)	+0.044(93)	+0.894(28)	+0.088(41)
$(65.2°, 158°)$	+0.002(58)	+0.931(07)	+0.000(60)	+0.920(10)	+0.049(33)	+0.847(32)
$(88.2°, 161°)$	−0.727(23)	+0.158(07)	−0.701(28)	+0.143(05)	−0.671(42)	+0.135(50)
$(71.7°, 133°)$	−0.818(13)	+0.505(18)	−0.813(14)	+0.500(19)	−0.772(23)	+0.553(23)
$(89.1°, 136°)$	−0.921(03)	+0.052(03)	−0.913(04)	+0.046(02)	−0.909(26)	+0.033(35)

from the simulation are based on the uncertainty of the polarization of the incident photon beam, for the FEA values, additionally uncertainties in the scattering angles $\Delta\theta = 0.1°$ and $\Delta\phi = 1°$ are included. While the FEA should be best at the center of the Compton peak, still non-negligible differences to the simulation are visible, especially for non-zero azimuthal scattering angles $\phi \neq 0$. The experimental results are for most positions well in accordance with both values within the uncertainties, however being closer to predictions from the simulation.

The polarization of the Compton scattered radiation across the Compton peak is displayed in figure 7. For each scattering angle, the Stokes parameters and the degree of linear polarization of the scattered beam are shown over an energy range of −9 keV to +12 keV from the center of the Compton peak in steps of 3 keV. Additionally, the expected polarization characteristics resulting from the simulation is shown. For comparison, also the estimated polarization from the FEA is displayed. While no complete overlap between the data points and either model can be reached, the simulated polarization results in a better representation of the polarization for each scattering position. Especially for the degree of linear polarization, the experimental data hint to a depolarization towards the tails of the Compton peak, which is also expected by the simulation results.

In order to better elucidate the comparison between the experiment and calculations, the deviations of the measured polarization characteristics from both models (simulation and FEA) are shown in figure 8 for each analyzed data point shown in figure 7. For better comparison, the deviations are normalized to the uncertainties of the experimental data points. For both the FEA and the simulation, the mean of these

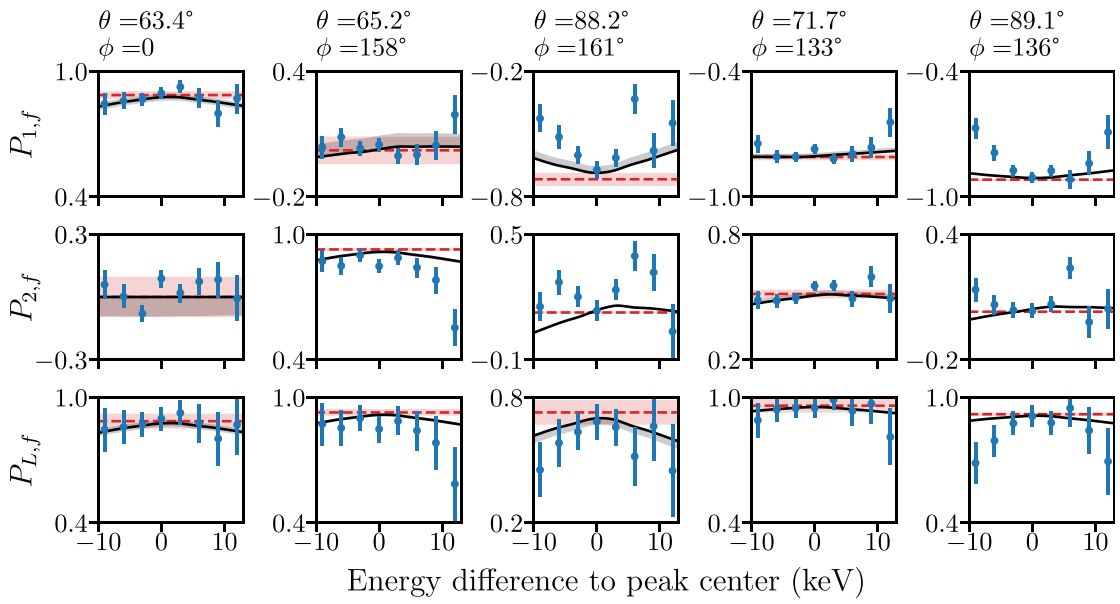

Figure 7. Polarization of the Compton scattered beam across the Compton peak. The experimental data (blue points with errorbars) are obtained in energy windows with a width of ±1.5 keV. The predicted Stokes parameters and degree of polarization from the simulation are indicated by the solid black lines. Additionally, the red lines show the polarization according to the FEA. The shaded areas show the uncertainties in the theory values.

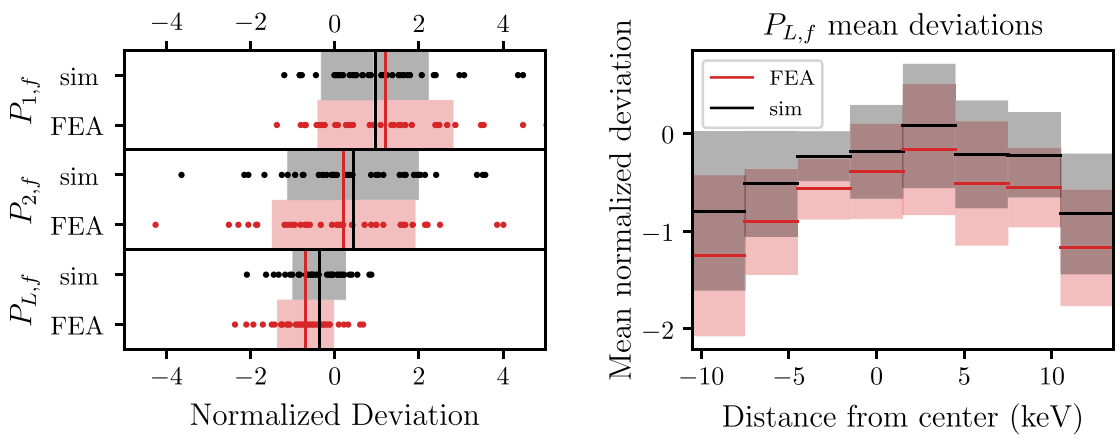

Figure 8. Left: Deviation of the measured polarization characteristics to both the FEA (red) and the simulation (black) normalized to the experimental uncertainties for each shown data point in figure 7. The vertical lines and shaded areas show the mean and standard deviation of the normalized deviation. Right: Mean normalized deviation for $P_{L,f}$ for each energy window.

deviations is non-zero. However, especially for the degree of linear polarization, the (absolute) mean of the deviations is smaller for the simulation. Additionally, the spread of the individual deviations, indicated by their standard deviation, is smaller for the model based on the simulation than for the FEA for all analyzed polarization characteristics. This confirms the better description of the polarization behavior by the simulation compared to the FEA.

The right plot in figure 8 shows for both models (FEA and simulation) the mean of the normalized deviation (from the measured values) for the degree of linear polarization resolved for each energy distance from the Compton peak center. While again the mean normalized deviation for the simulation is lower than for the FEA model for each energy difference, a clear systematic trend is visible, as for each energy distance the mean deviation is negative, meaning the measured linear polarization is lower than the predictions. This deviation is for the simulation almost non-existent around the center of the Compton peak and gets more pronounced for higher energy distances. An explanation for this trend is a background in the measured spectrum for which no correction was applied. From the fit of the Compton peak in figure 6, a non-zero background radiation is clearly visible. This background will also influence the polarization of the analyzed radiation and probably cause a depolarization. As the signal-to-noise ratio decreases towards the tails of the Compton peak, the background polarization will especially influence the measured polarization for these

regions leading to the stronger deviation here. However, since the polarization of the background is unknown, a correction for this small influence is not possible.

Assuming, that the simulation provides a correct representation of the polarization of the scattered beam, at least in the center of the Compton peak, the results provided in table 3 can be used to estimate the polarization of the incident photon beam. For this, $P_{1,i}$ and $P_{2,i}$ are adjusted in (9) for each position such, that $\mathbf{P_f}$ equals the experimental values. From the weighted mean of the individual results, the Stokes parameters for the incident radiation are $P_{1,i} = 0.9896 \pm 0.0063$ and $P_{2,i} = 0.012 \pm 0.018$. This result is in good agreement with a previous result from the experiment [23] and thus is a further confirmation of the validity of the simulation. Additionally, this shows, that depending on the spectral feature of interest (either the elastically or the inelastically scattered photons), the incident photon polarization can independently be determined based on the other spectral features of the scattered photons.

6. Conclusion and outlook

We have investigated the linear polarization of Compton scattering off bound electrons. For this purpose, we developed a Monte Carlo simulation of the Compton scattering process based on the concept of the IA. In this simulation, the three-dimensional electron momentum is taken into account and the scattering process is calculated in the electron rest frame using the transfer matrix formalism. The simulation provides the DDCS and the linear polarization of the scattered photon beam energy-resolved across the entire Compton peak. For the DDCS, a good agreement is found with an existing calculation based on the treatment proposed by Ribberfors especially for unpolarized incident photons. However, for scattering of a polarized incident photon beam off a high-Z target, our simulation shows a strong deviation from the existing model at the tails of the Compton peak, especially pronounced for scattering into directions, where the Klein–Nishina cross section is minimized. A special focus was set to the polarization transfer from incident to scattered photon across the Compton peak, this has not been thoroughly investigated so far, to the best of our knowledge. The simulation indicates a strong influence of the bound electron momenta on the polarization of the scattered photon beam. Especially the scattering off inner-shell electrons strongly deviates from Compton scattering off free electrons, even at the center of the Compton peak. This can especially be seen by the abrupt change in the linear polarization at the K-shell edge of the scattering atoms and can be attributed to the higher probability for high electron momenta in the stronger bound shells.

The findings of the simulation are also confirmed in a qualitative manner by experimental data from a measurement performed at beamline P07 of PETRA III @DESY. In this experiment a highly polarized hard x-ray beam with a photon energy of 175 keV was scattered off a thin gold target. The energy-resolved intensity profile of the scattered radiation was reproduced in a broad energy range by the simulated DDCS with only minor correction terms for the detector response. Additionally, the linear polarization of the Compton scattered radiation was investigated for certain photon energies across the Compton peak. In the center of the Compton peak, the linear polarization is in good agreement with both estimations from the FEA and the simulation based on the relativistic IA within the uncertainties. Across the Compton peak, the experimental findings indicate a change of the linear polarization, and in particular a decreasing degree of linear polarization as the photon energy gets further away from the center of the Compton peak. This behavior is well in accordance with our simulation. However, due to experimental limitations, only a small energy range of the entire Compton peak around the center was investigated in the experiment, while the strongest effects are expected at the far tails of the peak.

For a more thorough investigation of the polarization transfer in Compton scattering we propose multiple follow–up experiments. As it has been seen in the simulation, a sudden change in polarization is expected at the K-edge. Shifting the incident photon energy or using a different atomic target, the position of the K-edge can be changed such, that it moves in the energy range we are able to investigate. Another approach would be to investigate only Compton scattering off K-shell electrons. This could be done by a coincident detection of the fluorescent radiation from a K-shell vacancy. The question of whether effects beyond the IA have to be considered in the description of the Compton scattering on bound electrons, is out of the scope of this work and needs to be addressed in future.

Data availability statement

The data that support the findings of this study are openly available at the following URL/DOI: https://doi.org/10.5281/zenodo.15386614.

Acknowledgments

The authors acknowledge financial support from the German Federal Ministry of Education and Research (BMBF) under Grant No. 05P15SJFAA. W.M. acknowledges funding from BMBF via Verbundforschung Grant No. 05P19SJFAA. Support from the SPARC collaboration is acknowledged. Parts of this research were carried out at the light source PETRA III @ DESY, a member of the Helmholtz Association (HGF). Support in the preparation of the experiment from the GSI target laboratory, the GSI Department of Experiment Electronics and the Workshops of Friedrich Schiller University Jena is acknowledged. We thank Andrey Surzhykov, Anna Maiarova, Daniel Seipt and Jonas Sommerfeld for valuable discussions.

ORCID iDs

W Middents 0000-0001-8105-4657
A Gumberidze 0000-0002-2498-971X
T Krings 0000-0002-2212-7948
T Over-Winter 0000-0001-9737-3193
P Pfäfflein 0000-0003-0517-0722
N Schell 0000-0001-8238-341X
U Spillmann 0000-0001-7281-5063
G Weber 0000-0002-0833-8028
Th Stöhlker 0000-0003-0461-3560

References

[1] Compton A H 1923 *Phys. Rev.* **21** 483–502
[2] Compton A H 1923 *Phys. Rev.* **22** 409–13
[3] Klein O and Nishina T 1929 *Z. Phys.* **52** 853–68
[4] McMaster W H 1961 *Rev. Mod. Phys.* **33** 8–28
[5] Fano U 1949 *J. Opt. Soc. Am.* **39** 859
[6] Du Mond J W M 1929 *Phys. Rev.* **33** 643–58
[7] Du Mond J W M 1933 *Rev. Mod. Phys.* **5** 1–33
[8] Ribberfors R 1975 *Phys. Rev. B* **12** 2067–74
[9] Pratt R H, LaJohn L A, Florescu V, Surić T, Chatterjee B K and Roy S C 2010 *Radiat. Phys. Chem.* **79** 124–31
[10] Eisenberger P and Platzman P M 1970 *Phys. Rev. A* **2** 415–23
[11] Melzer N *et al* 2024 *Phys. Rev. Lett.* **133** 183002
[12] Surić T, Bergstrom P M, Pisk K and Pratt R H 1991 *Phys. Rev. Lett.* **67** 189–92
[13] Bergstrom P M, Surić T, Pisk K and Pratt R H 1993 *Phys. Rev. A* **48** 1134–62
[14] Qiao C K, Wei J W and Chen L 2021 *Crystals* **11** 525
[15] Middents W 2025 PACS - Polarization Transfer in Atomic Compton Scattering (https://doi.org/10.5281/zenodo.15386614)
[16] Koga T, Matsuyama H, Inomata H, Romera E, Dehesa J S and Thakkar A J 1998 *J. Chem. Phys.* **109** 1601–6
[17] Matsuyama H private communication
[18] Cocke W J and Holm D A 1972 *Nat. Phys. Sci.* **240** 161–2
[19] Eichler J and Stöhlker T 2007 *Phys. Rep.* **439** 1–99
[20] Salvat F and Fernández-Varea J M 2009 *Metrologia* **46** S112
[21] Ribberfors R and Berggren K F 1982 *Phys. Rev. A* **26** 3325–33
[22] Schell N, King A, Beckmann F, Fischer T, Müller M and Schreyer A 2013 *Mater. Sci. Forum* **772** 57–61
[23] Middents W *et al* 2023 *Phys. Rev. A* **107** 012805
[24] Vockert M, Weber G, Spillmann U, Krings T, Herdrich M O and Stöhlker T 2017 *Nucl. Instrum Methods Phys. Res. B* **408** 313–6
[25] Weber G *et al* 2012 *AIP Conf. Proc.* **1438** 73–79
[26] Lei F, Dean A J and Hills G L 1997 *Space Sci. Rev.* **82** 309–88
[27] Weber G *et al* 2015 *J. Phys.: Conf. Ser.* **583** 012041
[28] Weber G *et al* 2015 *J. Phys. B: At. Mol. Opt. Phys.* **48** 144031
[29] Blumenhagen K H *et al* 2016 *New J. Phys.* **18** 119601
[30] Hirayama H, Namito Y, Bielajew A F, Wilderman S J, Michigan U, Nelson W R, Arbor A and Nelson W R 2005 2005 *SLAC Report SLAC-R-730 and KEK Report 2005-8* 441
[31] Weber G, Bräuning H, Märtin R, Spillmann U and Stöhlker T 2011 *Phys. Scr.* **T144** 014034
[32] Dembinski H *et al* 2020 (https://doi.org/10.5281/zenodo.3949207)